

Journal of Materials Chemistry B

Materials for biology and medicine

Accepted Manuscript

This article can be cited before page numbers have been issued, to do this please use: F. Wu, Y. Liu, Y. Wu, J. Qian, D. Song and B. Zhu, *J. Mater. Chem. B*, 2020, DOI: 10.1039/C9TB02646K.



This is an Accepted Manuscript, which has been through the Royal Society of Chemistry peer review process and has been accepted for publication.

Accepted Manuscripts are published online shortly after acceptance, before technical editing, formatting and proof reading. Using this free service, authors can make their results available to the community, in citable form, before we publish the edited article. We will replace this Accepted Manuscript with the edited and formatted Advance Article as soon as it is available.

You can find more information about Accepted Manuscripts in the [Information for Authors](#).

Please note that technical editing may introduce minor changes to the text and/or graphics, which may alter content. The journal's standard [Terms & Conditions](#) and the [Ethical guidelines](#) still apply. In no event shall the Royal Society of Chemistry be held responsible for any errors or omissions in this Accepted Manuscript or any consequences arising from the use of any information it contains.

Chlorin e6 and polydopamine modified gold nanoflowers for combined photothermal and photodynamic therapy

Fengren Wu,^{a,b} Yongjia Liu,^b Yan Wu,^a Dianwen Song,^c Jiwen Qian^a and Bangshang Zhu^{*a,b}

Received 00th January 20xx,
Accepted 00th January 20xx

DOI: 10.1039/x0xx00000x

www.rsc.org/

Combinational photo-based approaches with enhanced efficacy for cancer therapy have garnered increasing attention in recent years. In this work, a multifunctional system for synergistic photothermal and photodynamic cancer therapy was successfully prepared. The system consists of gold nanoflowers (AuNFs) conjugated with Chlorin e6 (Ce6), and then coated with polydopamine (PDA) layer. The AuNFs with diameter around 80 nm and a broad absorbance in the visible–near infrared (Vis–NIR) range of 500 to 800 nm, were successfully synthesized by a two-step process at 0 °C, using HAuCl₄, ascorbic acid (AA), and hydroxylamine hydrochloride (NH₂OH·HCl) as the reactants. Glutathione (GSH) molecules chemically anchored to the gold surfaces were used to provide addressable sites for Ce6 conjugated to GSH–AuNFs through an amidation reaction. A PDA layer was then wrapped outside of the Ce6–GSH–AuNFs via self-polymerization of dopamine, which provided additional chemical modification and functionalization. Finally, the multifunctional PDA–Ce6–GSH–AuNFs were obtained. The content of Ce6 incorporated on the AuNFs was 14.0 wt. %, and the singlet oxygen yield of PDA–Ce6–GSH–AuNFs was approximately 91.0% of free Ce6. PDA–Ce6–GSH–AuNFs showed better photothermal conversion efficiency ($\eta = 23.6\%$), lower cytotoxicity, and faster cell internalization. Both *in vitro* and *in vivo* investigation of the combined treatment with near-infrared (NIR) laser (660 nm for photodynamic therapy, and 808 nm for photothermal therapy) demonstrated that PDA–Ce6–GSH–AuNFs had excellent phototoxicity and synergistic effects of killing cancer cells. Hence, PDA–Ce6–GSH–AuNFs is a dual phototherapeutic agent that exhibits photodynamic and photothermal therapeutic effects and has potential application in enhanced cancer therapy.

Introduction

Cancer is a major threat to human health, and its treatment remains one of the major health concerns in the present time and the future. At present, radiotherapy, chemotherapy, immunotherapy, and operative treatment are the main therapies.¹ These treatments inevitably damage normal cells and have major side effects causing significant pain to patients. Therefore, safe and efficient cancer therapies are an important topic for both researchers and patients.² Photodynamic therapy (PDT) is a form of phototherapy involving photosensitizers (PSs) and light irradiation, which produces phototoxicity to elicit cell injury and cell death. It is used clinically to treat a wide range of cancers and non-neoplastic diseases with minimal side effects.³ The treatment process involves the aggregation of PSs in the tumour tissues and irradiation with an appropriate wavelength of light to

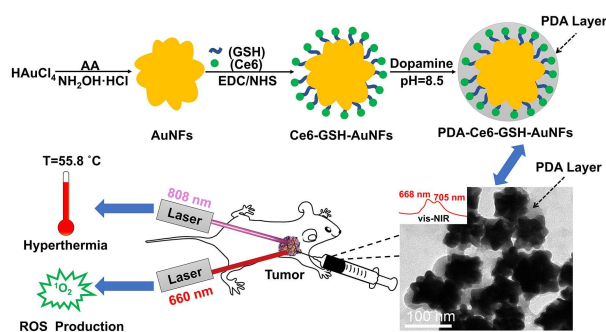
generate reactive oxygen species known as singlet oxygen (¹O₂) that can kill malignant cells or tissues.⁴ PDT is considered as a powerful non-invasive therapeutic technique for localized cancers with minimum damage to the surrounding normal cells. Compared with traditional therapies, PDT is safe, efficient, repeatable, and less invasive.^{5,6} Furthermore, photothermal therapy (PTT) is an extension of PDT, in which PSs are excited with a specific band light. Unlike PDT, PTT does not require oxygen to interact with the target cells or tissues, in which near-infrared (NIR) photon energy is converted into heat to kill target cells.⁷ It has been developed as an alternative reduced invasiveness option for the local destruction of cancer cells. Over the last ten years, different nanomaterials based on PTT have been developed that have the capability for targeted therapy using NIR light.⁸ Furthermore, PTT can overcome some disadvantages of conventional hyperthermia, which is non-selective in tissue heating and causes serious side effects.⁹ During the process of PDT, the light-absorbing agents, which are also referred to as photothermal agents, can absorb and transfer the energy from NIR light onto the tumour to produce localized thermal destruction,¹⁰ thereby reversing the direction of heat loss (inside–out hyperthermia) and minimizing the adverse effects on healthy tissues. Recently, a combination therapy involving PTT and PDT based on nanostructures was considered as a promising

^a School of Chemistry and Chemical Engineering, Shanghai Jiao Tong University, Shanghai 20040, China. E-mail: bshzhu@sjtu.edu.cn

^b Instrumental Analysis Center, Shanghai Jiao Tong University, Shanghai, 20040, China

^c Department of Orthopedics, Shanghai General Hospital, School of Medicine, Shanghai Jiao Tong University, Shanghai, 201620, China.

† Electronic Supplementary Information (ESI) available: [details of any supplementary information available should be included here]. See DOI: 10.1039/x0xx00000x



Scheme 1 The illustration of the preparation procedure of PDA-Ce6-GSH-AuNFs and used for synergistic PTT and PDT *in vitro* and *in vivo*.

cancer treatment, in which multiple components such as photothermal energy transducers and PSs were used for the synergistic effects.⁸ Wang et al. developed a simple strategy for simultaneous synergistic PDT/PTT treatment. In their study, transferrin was chosen as a drug carrier to load IR780 iodide which could destroy cancerous cells *in-vitro* and *in-vivo* via its photosensitizing properties.¹¹ Zhang et al. designed a PTT and PDT agent in combination with chemotherapy and adjuvant immunotherapy and had a remarkable synergistic therapeutic outcome in gastric carcinoma.¹² Pang et al. reported a kind of nanoscale porphyrin-containing covalent organic polymer that showed high antitumor efficacy when combined with PTT and PDT.¹³

Compared with the first-generation PSs, Chlorine e6 (Ce6) is regarded as a promising second-generation PS with improved efficacy and decreased side effects because of its high singlet oxygen generation capability.¹⁴ Even though Ce6 had some success in PDT therapeutic cancers, like most other PSs, it has some limitations such as water insolubility and difficulty to inject intravenously.¹⁵ To solve the problem, the development of drug delivery system for PSs would be a prospective approach. One way is to conjugate the PSs with receptors. As reported by Xu et al.,¹⁶ zinc phthalocyanine was added to gonadotropin-releasing hormone receptors to enhance the selectivity of PSs. Furthermore, constructing nanoparticles as a multifunctional platform is in favour of the delivery of PSs. Yan et al. synthesized a polydopamine (PDA)-based carrier with modified folic acid to load a cationic phthalocyanine-type PS with high efficiency and specificity.¹⁷ Jia et al. reported a self-assembled pentalyisine-phthalocyanine nanodot as a nanoparticle platform to solve the problem of off-target photodynamic effects.¹⁸

Among most nanoparticles, gold nanoparticles (AuNPs) have emerged as a promising platform for PDT, and have been widely used to deliver PS agents for cancer treatment.¹⁹ The adjustable surface plasmon resonance (SPR) band from visible (Vis) to NIR region of AuNPs allows their optical extinction to be tuned to match the irradiation wavelengths of common NIR lasers using in optical imaging and therapy.²⁰ Their strong optical absorption allows photothermal conversion that facilitates photothermal therapy and laser-triggered drug release.²¹ *In vitro* studies have demonstrated that the Au-Ce6 conjugates performed with both of photophysical and photochemical

destructions to cancer cells, thereby significantly enhancing the efficacy of treatment compared with a single treatment of PDT or PTT. Gold nanorods have an increased yield of singlet oxygen due to the enhancement of events such as triplet yield, and photostability of PSs.²² In addition to gold nanorods, gold nanoshells, nanovesicles, and nanoclusters were also modified with Ce6 to improve the PDT effects of cancer therapy.^{23–25}

Gold nanoflowers (AuNFs) are anisotropic gold nanomaterials with a flower-like morphology and branch structures. Compared with spherical, rod-shaped, or other shaped gold nanoparticles, AuNFs has a larger surface-area-to-volume ratio and high tissue penetration.²⁶ In reports on AuNPs, the loading content of Ce6 was not sufficiently high (approximately 6 wt. %).^{23,27} Thus the loading efficiency of Ce6 remains need to be improved, which would result in an improved PDT. AuNFs has tunable Vis–NIR absorbance similar to that of gold nanorods. They have wide application in biomedicine such as medicine carrying, imaging, and therapy.^{28–31} They can also effectively transfer laser energy to generate heat for photothermal therapy (PTT).³² Therefore, the combination of PDT and PTT can be realized through Ce6-loaded AuNFs.

Polydopamine (PDA) is the primary pigment in naturally occurring melanin (eumelanin). A macromolecule containing a constitutional unit consisting of catechol, an amine, and an imine, it can scavenge radicals, absorb ultraviolet rays, exhibit excellent adhesive properties, and exhibit photothermal conversion ability.³³ The strong NIR absorbance and high energy conversion efficiency of PDA make it an excellent photothermal agent. It is also often used as a biomaterial coated on substrate surfaces to improve biocompatibility. Surface modification with PDA depends on similar catecholamine functional groups, which provide the adhesiveness to form organic nanoscale thin films with low toxicity and high chemical and thermal stability on material surfaces.^{34,35} Coating a surface with a thin PDA layer (tens of nm) confers hydrophilicity and zwitterionic properties that enhance mucopenetration and cell uptake of nanoparticles as well as promoting hydrophobic drug delivery.^{36,37} Additionally, PDA coatings can result in a red-shift adsorption, which would enhance the photothermal transfer efficiency of the light-absorbing nanoparticles.³⁸

Herein, we provide a combined PTT and PDT nanoscale tumour therapy platform, in which AuNFs conjugated with Ce6 through the linkage of glutathione (GSH) and coated with nano-layered PDA. The system was designated and described as PDA-Ce6-GSH-AuNFs. It has the following characteristics: (i) strong absorbance in Vis–NIR range of 500–900 nm with enhanced photothermal conversion efficiency (23.6%); (ii) high loaded quantities of Ce6 (approximately 14.0 wt. %); (iii) faster cell internalization; and (iv) synergistic therapeutic effects of PTT and PDT. The entire preparation process is briefly described in Scheme 1. The morphology, particle size, and Vis–NIR absorbance of the AuNFs were optimized by the addition of a reducing agent and the optimizing the reaction temperature. The Ce6 loading content and the generated singlet oxygen were measured to verify the drug loading capacity. The photothermal performance was tested to determine the photothermal efficiency. Both *in vitro* and *in vivo* synergistic therapeutic effects of PTT and PDT

for cancer therapy were evaluated compared with individual PTT or PDT alone.

Materials and methods

Materials

Gold chloride trihydrate ($\text{HAuCl}_4 \cdot 3\text{H}_2\text{O}$, 99.9%), potassium carbonate (K_2CO_3), 1-(3-Dimethylaminopropyl)-3-ethylcarbodiimide hydrochloride (EDC) and Chlorin e6 (Ce6) were purchased from Sinopharm Chemical Reagent Co., Ltd (Shanghai, China). Hydroxylamine hydrochloride ($\text{NH}_2\text{OH} \cdot \text{HCl}$), ascorbic acid (AA), GSH, N-Hydroxysuccinimide (NHS), Tris(hydroxymethyl)aminomethane (Tris), hydrochloric acid (HCl , 37%), dopamine hydrochloride ($\text{DA} \cdot \text{HCl}$), 9,10-anthracenediylbis (methylene) dimalononic acid (ABDA), 3-(4,5-dimethylthiazol-2-yl)-2,5-diphenyltetrazolium bromide (MTT) and Hoechst 33342 were obtained from Sigma-Aldrich (St. Louis, MO, USA). All reagents and solvents employed were commercially available and used as received without further purification.

Synthesis of AuNFs

AuNFs were synthesized by a template-free method. The glassware used in the reaction was soaked in freshly prepared aqua regia and then rinsed several times with ultrapure water before oven-drying. HAuCl_4 (25 mL, 0.25 mM) and K_2CO_3 (1 mL, 0.2 M) were added to a 100 mL round-bottom flask. Next, AA (10 μL , 5 mM) was added to the solution to generate gold seeds. The colour of the solution quickly turned from light yellow to colourless. After stirring for 5 min, $\text{NH}_2\text{OH} \cdot \text{HCl}$ (1 mL, 10 mM) was added into the mixture rapidly. Furthermore, the colour turned from colourless to dark blue at once. The reaction was allowed to proceed for 10 min to ensure a complete reaction. The whole process occurred under vigorous stirring. The AuNFs were then centrifuged at 4000 rpm for 8 min, and the supernatant removed. The precipitates were washed three times and redistributed in 2.5 mL ultrapure water. Finally, they were kept at 4 °C until used.

To explore the optimum AuNFs synthesis temperature conditions, the reaction were performed at 0, 10, 20 and 40 °C. After that, the size of the AuNFs determined by the concentration of Au seeds were investigated, which closely related to the amount of reducing agent AA. Under the reaction temperature of 0 °C and constant reaction volume, the AA addition with 5, 10, 15, and 20 μL were examined.

Synthesis of PDA-Ce6-GSH-AuNFs

GSH-AuNFs. 7.5 mL AuNFs contained solution and 12.5 mL ultrapure water were added to a 100 mL round-bottom flask, deaerated by pure nitrogen (>99%). Twenty min later, GSH (5 mL, 0.15 M) was injected into the flask. After stirring for 12 hours, the solution was dialyzed (8 kDa MWCO) for 6 h in ultrapure water. The nanoparticles precipitated and were re-dispersed in 7.5 mL of 50 mM phosphate-buffered saline (PBS, pH = 6.2).

Ce6-GSH-AuNFs. 5 mg Ce6 was diluted in 500 μL dimethyl sulfoxide (DMSO) and 9.5 mL PBS (pH = 6.2) until it dissolved

completely. Next, the solution was mixed with 60 mg EDC and 40 mg NHS. After stirring for 40 min, 5 mL GSH-AuNFs was injected into the mixture and stirred for another 24 h in the dark. Subsequently, the reaction was terminated by the dropwise addition of 0.1 M HCl until the pH value was adjusted to 1.0. Subsequently, the product was suspended in 5 mL ultrapure water then centrifuged at 6000 rpm for 15 min. The supernatant was collected for quantitative analysis the unconjugated Ce6.

PDA-Ce6-GSH-AuNFs. 5 mL ultrapure water was added to 5 mL Ce6-GSH-AuNFs and then 121.14 mg Tris and 12 μL HCl was mixed with the solution to set the pH to 8.5. Subsequently, 2.5 mg $\text{DA} \cdot \text{HCl}$ was added, and the solution stirred for six h. The desired product was centrifuged at 6000 rpm for 10 min and washed three times. It was stored at 4 °C for future use.

Physicochemical characterization

The Vis-NIR absorption of AuNFs, GSH-AuNFs, Ce6-GSH-AuNFs, and PDA-Ce6-GSH-AuNFs were acquired in the region of 300–1000 nm by UV-Vis spectroscopy (Nicolet Evolution 300, Thermo Scientific, USA) in a 10-mm quartz cuvette. X-ray diffraction (XRD) patterns were obtained with a poly-functional x-ray diffractometer (3kW/*D8 Advance Da Vinci, Bruker, Germany) using Cu K α (0.15405 nm) with a scan rate (2 θ /s) of 0.02°/s, and the scan range (2 θ) of 10–90°. Dynamic light scattering (DLS) and Zeta potential were measured by particle size and Zeta potential analyzer (NanoBrook Omni, Brookhaven, USA). Through a transmission electron microscope (TEM) (Tecnai G2 spirit Biotwin, FEI, USA), the morphology and size of the nanoparticles were investigated. The selected area electron diffraction and high-resolution transmission electron microscopy were performed on a field emission transmission electron microscope (FE-TEM, Talos F200X, FEI, USA). The surface-modified components on the nanoparticles were characterized by Fourier transform infrared spectroscopy (FTIR) (Nicolet 6700, Thermo Fisher, USA). The FTIR analyses were carried out in the range of 400–4000 cm^{-1} using transmission mode.

Ce6 loading and *in vitro* release

The loading content of Ce6 was measured by UV-Vis spectroscopy. The calibration curve (Fig. S9A) was obtained through the measurements with Ce6 concentrations of 5, 10, 20, 50 and 100 $\mu\text{g}/\text{mL}$. The unconjugated Ce6 in the supernatant during the preparation of PDA-Ce6-GSH-AuNFs was quantified through the UV-Vis calibration curve of Ce6 at 656 nm. The loading content of Ce6 was evaluated by thermo-gravimetric analysis (TGA) (Pyris 1 TGA, Perkin Elmer, USA), under nitrogen-flow (100 mL/min), recording data from 25 to 900 °C at a heating rate of 20 °C/min.

To evaluate Ce6 release *in vitro*, PDA-Ce6-GSH-AuNFs, and Ce6-GSH-AuNFs solution was adjusted to 1 mg/mL, and added into dialysis tubes (8 kDa MWCO), immersed in 30 mL of PBS solutions of different pH (5.8, 6.5 and 7.4) and shook (100 rpm) at 37 °C. The concentration of released Ce6 at different set times was measured by UV-Vis spectroscopy, and the cumulative release mass was calculated. The experiments were repeated three times.

Singlet oxygen generation assay

ABDA, a trapping agent for the singlet oxygen of PSs, was employed to test the generation capability of $1O^2$ by UV-Vis spectroscopy at 400 nm in a 10-mm quartz cuvette. Ce6 and PDA-Ce6-GSH-AuNFs were mixed with 3 mL ABDA (0.25 mM). The solutions were irradiated with a NIR laser (660 nm, 100 mW/cm²) for 2.5, 5, 7.5, 10, 12.5, 15, 17.5, 20, 22.5 and 25 min. The sample solutions were then measured by UV-Vis spectroscopy, and the profiles of singlet oxygen generation were obtained.

Measurement of photothermal performance

Two mL of 200 µg/mL of AuNFs, and PDA-Ce6-GSH-AuNFs in PBS (pH = 7.4) were prepared in a 10-mm quartz cuvette to evaluate the photothermal effect of AuNFs. Two mL PBS (pH = 7.4) served as a control. Each sample was irradiated with an 808 nm laser (2 W/cm²), and thermal variation was determined by measuring the change of temperature every 2 min with a Thermal infrared imager (Ti125, Fluke, USA).

Cell culture

L929 healthy cells and HeLa cancer cells, both purchased from BeNa Culture Collection (Shanghai, China), were cultivated in Dulbecco's modified Eagle's medium (DMEM) (Life Technologies, UK) containing 1% antibiotics (50 units/mL streptomycin and 50 units/mL penicillin) and 10% fetal bovine serum (FBS). The cells were cultivated at 37 °C with a humidified atmosphere containing 5% CO₂.

Cell uptake of PDA-Ce6-GSH-AuNFs examined by CLSM

The HeLa cells were seeded in a 24-well plate at 7.5×10^4 cells per well in 0.5 mL DMEM with coverslips cultured for 12 h in a humidified atmosphere containing 5% CO₂. The cells were cultured in 0.5 mL of DMEM containing PDA-Ce6-GSH-AuNFs at the Ce6 concentration of 10 µg/mL, incubated for different time intervals (15, 30, 60 and 120 min) and then rinsed three times with PBS. Subsequently, the cells were fixed with 4% paraformaldehyde for 20 min and after that rewashed with PBS. The fixed cells were stained with Hoechst 33342 (10 µg/mL) for 10 min, then rinsed three times with PBS. The coverslips were immersed in ultrapure water for a few seconds and put on glass microscope slides. Finally, fluorescence images of the cells were examined with confocal laser scanning microscopy (CLSM, TCS SP8 STED 3X, Leica, Germany).

TEM observation of PDA-Ce6-GSH-AuNFs treated HeLa cells

HeLa cells were seeded in a 6-well plate at a density of 2.0×10^6 cells per well and incubated for 24 h. After attachment, cells were incubated with PDA-Ce6-GSH-AuNFs (50 µg/mL) in 10 mL of fresh medium for four h, washed three times with PBS, and fixed with 2.5% glutaraldehyde overnight. After additional post-treatment, the morphology of AuNFs in HeLa cells was examined by transmission electron microscopy (TEM, Tecnai G2 Spirit Biotwin, FEI, USA).

In vitro cytotoxicity assay

The L929 cells and HeLa cells were seeded into 96-well plates at 1.0×10^4 cells per well in 200 µL DMEM, and incubated for 24 h. The culture medium was then replaced by 200 µL DMEM containing several dilutions of AuNFs, Ce6-GSH-AuNFs, and PDA-Ce6-GSH-AuNFs. The cells were cultivated for 36 h. Subsequently, 20 µL of MTT assays stock solution (5 mg/mL) in PBS and 180 µL DMEM were added to each well and cultivated for another 4 h. The medium and unreacted MTT were then removed. The remaining formazan crystals were dissolved in 200 µL DMSO per well, shook for 15 min at room temperature, and then measured in a BioTek SynergyH4 at the wavelength of 490 nm.

Photothermal and photodynamic therapy *in vitro*

MTT assays were also used to study the cytotoxicity of PDA-Ce6-GSH-AuNFs, AuNFs, and free Ce6 using laser against the HeLa cells. During the experiment, HeLa cells were seeded in 96-well plate at a density of 1.0×10^4 cells per well for 24 h. The cells were then treated with fresh culture medium containing different doses of PDA-Ce6-GSH-AuNFs, AuNFs, and free Ce6, and incubating for 12 h. Subsequently, the cells were exposed to 808 nm laser (2 W/cm²) for 10 min (PTT irradiation), or 660 nm laser (100 mW/cm²) for 5 min (PDT irradiation), or the combination of the PDT/PTT irradiation (5 min for each), respectively. After laser irradiation, the cells were incubated with fresh DMEM for 24 h. The cell viability was then evaluated by MTT assay.

Evaluation of photodynamic/photothermal therapy *in vivo*

Twenty-five female BALB/c mice (6 weeks old) were purchased from Shanghai Slac Laboratory Animal Co. Ltd. All animal operations were performed per institutional regulations for animal use and care of Shanghai Jiao Tong University (Approval No: A2019032). A suspension of 1.0×10^7 HeLa cells in 100 µL phosphate-buffered saline (PBS) was subcutaneously administered into the flank of each mouse. When their tumour size reached approximately 80 mm³, PDA-Ce6-GSH-AuNFs (40 µL, 2 mg/mL) were injected intratumorally. The mice were segregated into five groups:

- (1) Sterilized PBS without laser irradiation ($n = 5$);
- (2) PDA-Ce6-GSH-AuNFs without laser irradiation;
- (3) PDA-Ce6-GSH-AuNFs were subjected to single laser irradiation under 808 nm (2 W/cm²) for 10 min;
- (4) PDA-Ce6-GSH-AuNFs were subjected to single laser irradiation under 660 nm (100 mW/cm²) for 10 min;
- (5) PDA-Ce6-GSH-AuNFs were subjected to combined laser irradiation under 660 nm (100 mW/cm²) and 808 nm (2 W/cm²) simultaneously for 10 min.

The NIR laser irradiation was conducted 24 h after injection. The therapeutic effects were evaluated by monitoring the tumour volume and body weight changes in each group every 2 days, up to 14 days. The tumour size was measured using callipers every other day after the treatment. Meanwhile, the histological changes of the tumours were examined at the end of the treatment cycle, one tumour-bearing mouse in each group was stained with

Haematoxylin and eosin (H&E) for histopathology evaluation and Ki67 antibody for immunohistochemical analysis.

Statistical analysis

All statistical analysis was performed by one-way analysis of variance (ANOVA) and LSD treatment using SPSS 17.0 (SPSS Inc., Chicago, IL). The statistical significance was set at $P < 0.05$ (*) and $P < 0.001$ (**), respectively. The results were expressed as mean \pm standard deviation (SD).

Results and discussion

Size, morphology and Vis–NIR spectra of AuNFs

AuNFs were synthesized through a template-free method, which involving two steps without surfactant.³⁹ They would have abundant branches under the reaction temperature of 0 °C, while the size (approximately 60–100 nm) of particles could be well controlled by adjusting the dosage of the reducing agent AA.

During the synthesis process, the Au seeds were firstly prepared, in which the Au precursor (HAuCl₄) was reduced with AA. The branched gold nanoparticles were formed by seed-mediated approach in the second step, in which Au³⁺ was reduced to Au⁰ by NH₂OH·HCl while Au was deposited on crystal nucleus (Au seeds) to form AuNFs. Consequently, the multi-branched AuNFs were obtained. In order to modulate the morphology and particle size of the AuNFs, the reaction conditions including the reaction temperature and the 1st reducing agent (AA) amount were investigated. It was found that the particle morphology and size, and the branched degrees of AuNFs could be well-controlled by modulating the reaction temperature and the amount of reducing agent AA. AuNFs were synthesized at the temperature of 0, 10, 20, 30 and 40 °C, respectively. When the temperature rise from low to high, the nanoparticle morphology changed as well (Fig. S1A, ESI†). The temperature was a key parameter influencing the final morphology of AuNFs. When the reaction temperature increases, the branched spikes grew fewer until almost completely disappeared. Low temperature was favourable for the growth of branched structures, and 0 °C was the optimal reaction temperature to achieve AuNFs with many elongated spikes. This phenomenon might be attributed to the slow diffusion rate of Au ions on the Au seed particle surface under the lower temperature, which result in the generation of highly branched AuNFs. When the process was performed under higher temperatures, the high growth rate of AuNFs results in a larger size.⁴⁰ Accordingly, the Vis–NIR absorbance ranged from 500 to 800 nm (Fig. S1B, ESI†), and the maximum absorption peak of the AuNFs synthesized at 0 °C was 616 nm. In addition, the size of gold nanoflowers that obtained at the reaction temperature of 0, 10, and 20 °C was similar. However, their Vis–NIR absorption peak was quite different, which was due to the difference of branched structures, and the maximum absorption peak red-shifted to the near-infrared region.⁴¹

The amount of 1st reducing agent AA affected the ratio of the number of formed gold seeds per unit volume in the reaction solution, and hence the number of gold crystal nucleus determine

the finally size of AuNFs. When the amount of added AA decreased in turn from 20, 15, 10 and 5 μ L, the size of AuNFs increased from ~60 nm to ~100 nm, as shown in Fig. S2A (ESI†), while the morphology of AuNFs seldom changed. Furthermore, the surface plasmon resonance or Vis–NIR absorption of the AuNFs is size-dependent. The red-shift of the absorption increased as the gold nanoparticle size increased, as illustrated in Fig. S2B (ESI†). The absorption peak shifted from 575 nm to 652 nm. In concern of good cell uptake of particles below 100 nm,^{20,42} We chose AuNFs prepared at 0 °C using the first reducing agent AA (10 μ L, 5 mM) for subsequent experiments. The particles were about 80 nm in size, and the Vis–NIR absorption was 616 nm.

Physicochemical characterization of PDA-Ce6-GSH-AuNFs

To obtain the PDA-Ce6-GSH-AuNFs, we first conjugated GSH on the surface of AuNFs synthesized at 0 °C. The thiol group of GSH is easily bonded on the surface of the AuNFs via stable Au–S bond.^{43,44} Thus, GSH used as a linker was conjugated on the surface of AuNFs. EDC and NHS were then added to activate the carboxyl groups of GSH. Subsequently, the amino groups of Ce6 reacted with the activated carboxyl groups, and Ce6-modified AuNFs were successfully prepared. Finally, dopamine undergo in-situ polymerization to form PDA in a weak alkaline solution (pH = 8.5), PDA layer was wrapped on the surface of the Ce6-GSH-AuNFs, and PDA-Ce6-GSH-AuNFs was obtained.

According to the XRD pattern of the AuNFs shown in Fig. 1A, there are five peaks at 38.28°, 44.56°, 64.77°, 77.84° and 81.93°, corresponding to the (111), (200), (220), (311) and (222) planes of the face-centered-cubic gold respectively.⁴¹ High-resolution transmission electron microscopy (HRTEM) images demonstrate that protrusions with a random orientation derived from the solid dark core are crystalline (Fig. S3A, ESI†),³⁹ while the selected area electron diffraction (SAED) images (Fig. S3B, ESI†) further proved the polycrystalline character of the AuNFs. The energy dispersive spectrum (EDS) for elemental analysis confirmed the presence of an organic layer outside the PDA-Ce6-GSH-AuNFs (Fig. S3C, ESI†).

Fig. 1B shows the results of the TEM investigations of AuNFs, GSH-AuNFs, Ce6-GSH-AuNFs, and PDA-Ce6-GSH-AuNFs, from which the morphologies of AuNFs were found to be almost the same, and the PDA layer was approximately 10.2 nm in thickness. The dynamic light scattering analysis data indicated that the hydrodynamic diameter of GSH-AuNFs was 109.26 ± 6.72 nm (Fig. S4, ESI†), a little larger than AuNFs (83.75 ± 3.92 nm), and the hydrodynamic diameter of Ce6-GSH-AuNFs increased to 217.09 ± 5.38 nm. After the surface loaded with Ce6, growth of the diameter of Ce6-GSH-AuNFs was about 125 nm compared with that of bare AuNFs. The increasing size of Ce6-GSH-AuNFs is attributed to two reasons: the conjugation of GSH and Ce6, and the formation of a double-layer thickness due to the amine and carboxyl groups of the two organics.⁴⁵ After modification with PDA, the diameter of PDA-Ce6-GSH-AuNFs increased to 257 ± 8.67 nm. Since PDA has water binding affinity, PDA-Ce6-GSH-AuNFs became more hydrated and swellable in aqueous solution, and the hydrodynamic diameter increased.³⁶ The size distribution of four different nanoparticles

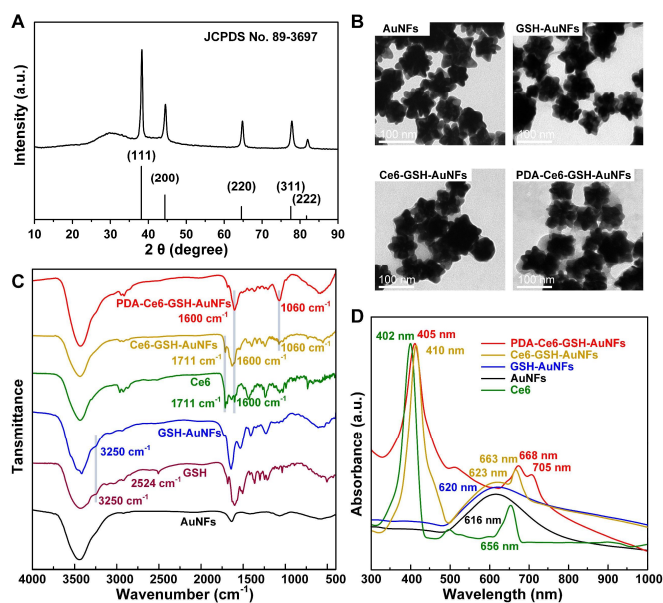


Fig. 1 Physicochemical characterizations of AuNFs or functionalized AuNFs. (A) XRD pattern of AuNFs. (B) TEM investigation of AuNFs, GSH-AuNFs, Ce6-GSH-AuNFs and PDA-Ce6-GSH-AuNFs. (C) FTIR spectra characterization of Ce6, GSH, AuNFs, GSH-AuNFs, Ce6-GSH-AuNFs and PDA-Ce6-GSH-AuNFs. (D) Vis-NIR absorbance of the Ce6, AuNFs, GSH-AuNFs, Ce6-GSH-AuNFs and PDA-Ce6-GSH-AuNFs.

was shown in Fig. S5 (ESI[†]). Moreover, the Zeta potential of nanoparticles changed with different nanoparticles. As shown in Fig. S4 (ESI[†]), for the adsorption of chloride ions from NH₂OH·HCl on the surface of AuNFs, the Zeta potential of AuNFs was -27.64 ± 1.98 mV.⁴⁶ After modification with GSH, the Zeta potential changed to -9.27 ± 2.47 mV. Owing to the amine groups' protonating and two carboxyl groups deprotonating of GSH at a neutral pH, GSH-AuNFs carried a negative charge.⁴⁷ The Zeta potential of Ce6-GSH-AuNFs was -22.4 ± 2.38 mV with three carboxyl groups deprotonating at pH > 5, which indicates the modified nanoparticles were electrostatically stable with the negative charges.⁴⁸ The Zeta potential of the PDA-Ce6-GSH-AuNFs was -17.36 ± 3.51 mV. Similarly, since the phenolic hydroxyl groups of PDA were deprotonated, the Zeta potential was also negative.⁴⁹

The FTIR spectra of different samples were also examined in comparing with AuNFs, GSH, and Ce6 (Fig. 1C) to verify the successful synthesis of PDA-Ce6-GSH-AuNFs. As shown in IR spectra, the most significant difference between AuNFs and GSH-AuNFs was the disappearance of the characteristic absorption peak at 2524 cm⁻¹, which is attributed to the vibration of S-H. Thus, the formation of the Au-S bond and conjugating of GSH onto the gold surface via the thiol group of Cys was confirmed. Meanwhile, there was a shoulder peak at 3250 cm⁻¹ due to the N-H stretching vibration of GSH. Ce6-GSH-AuNFs showed peaks of Ce6 at 1600 cm⁻¹, which is attributed to the vibration of the pyrrole rings.^{50,51} Furthermore, the C=O stretching peak of carboxylic acid at 1711 cm⁻¹ became stronger compared with GSH-AuNFs, which was the result of a combination between GSH and Ce6. Compared with Ce6-GSH-AuNFs, PDA-Ce6-GSH-AuNFs showed a sharp peak at 1600 cm⁻¹ corresponding to phenyl C=C stretching, which represents

the dopamine polymerization, and the peak at 1060 cm⁻¹ relates to the N-H shearing vibrations.⁵² The results of the FTIR spectra further confirmed the successful preparation of PDA-Ce6-GSH-AuNFs.

Fig. 1D shows the UV-Vis spectra of bare AuNFs, free Ce6, GSH-AuNFs, Ce6-GSH-AuNFs, and PDA-Ce6-GSH-AuNFs. The free Ce6 has two absorbance peaks at 402 nm and 656 nm. With respect to Ce6-GSH-AuNFs, the maximum absorption peak of the AuNFs red-shifted from 616 nm to 623 nm after GSH and Ce6 modification. Meanwhile, the NIR absorbance peak of Ce6 also has a small red-shift from 656 nm to 663 nm. PDA-Ce6-GSH-AuNFs shows a strong absorbance in the range of 500-900 nm, and there are two peaks at 668 and 705 nm, respectively. The former peak is attributed to the characteristic peak of Ce6, and the latter peak is originated from the red-shift of AuNFs after coated with a thin PDA shell layer. These results further proved the successful preparation of PDA-Ce6-GSH-AuNFs, and the particles possess two absorption peaks in the NIR region.

Additionally, the stability of PDA-Ce6-GSH-AuNFs in PBS (pH = 5.8) and FBS were evaluated. Even the concentration of PDA-Ce6-GSH-AuNFs in solution increased to 200 μg/mL, the particles showed well-dispersed in PBS (pH=5.8) or FBS, shown in Fig. S6 (ESI[†]). According to Fig. S7-8 (ESI[†]), there was no obvious measurable difference in size distribution and Vis-NIR absorption of PDA-Ce6-GSH-AuNFs between the 0-day group and the 7-day group. These results demonstrated that the stability of PDA-Ce6-GSH-AuNFs in PBS and FBS, which also means the merits of applications *in vivo*.

Loading content of Ce6

Due to the broad absorption range of AuNFs, it is difficult to directly measure the absorption of PDA-Ce6-GSH-AuNFs at 400 nm or 660 nm and obtain the content of Ce6. The loading amount of Ce6 was calculated by subtracting the amount in the supernatant (unloaded) from the feed amount. In the calibration curve, the absorption intensity was linearly dependent on the concentration of Ce6 shown in Fig. S9A (ESI[†]), and the regression linear equation was $y = 0.0864 + 0.00459x$, with $R^2=0.99758$. Using the equation, the content of Ce6 conjugated with GSH was determined to be 13.9 wt. % in PDA-Ce6-GSH-AuNFs.

GSH-AuNFs, Ce6-GSH-AuNFs, and PDA-Ce6-GSH-AuNFs were then evaluated by TGA analysis to further quantify the loading content of Ce6 and the amount of PDA. As shown in Fig. S9B and Tab. S1 (ESI[†]), the result of Ce6 was about 13.6% at 500 °C and 14.0 wt. % at 900 °C, which was close to the 13.9% determined by UV-Vis absorption spectra. The two methods got similar results, which means that mediated by GSH, there was approximately 14.0 wt. % Ce6 loaded onto the AuNFs.

Singlet oxygen generation and drug release study of PDA-Ce6-GSH-AuNFs

ABDA was used as an indicator showing that the decrease of ABDA at 400 nm to demonstrate the generation of singlet oxygen. As shown in Fig. 2A, the samples of PDA-Ce6-GSH-AuNFs and Ce6 were mixed with ABDA, respectively. Throughout the whole process, singlet oxygen produced by

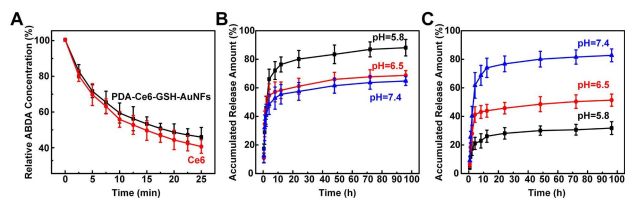


Fig. 2 (A) Singlet oxygen generation of PDA-Ce6-GSH-AuNFs and Ce6 mixed with ABDA respectively, and irradiated by a 660 nm laser (100 mW/cm^2) for 0, 2.5, 5, 7.5, 10, 12.5, 15, 17.5, 20, 22.5 and 25 min (mean \pm SD, $n = 3$). *In vitro* Ce6 release profiles of (B) Ce6-GSH-AuNFs and (C) PDA-Ce6-GSH-AuNFs in PBS solution at pH 5.8, 6.5 and 7.4 with time intervals of 1, 2, 4, 8, 12, 24, 48, 72 and 96 h (mean \pm SD, $n = 3$).

PDA-Ce6-GSH-AuNFs was $91.0\% \pm 2.5\%$. In comparing with that produced by Ce6, it was a little lower. This consequence might result from energy transfer and quenching effect between AuNFs and Ce6 for both absorption peaks around 660 nm.⁴⁸

The behaviour of Ce6 released from PDA-Ce6-GSH-AuNFs and Ce6-GSH-AuNFs was examined under different pH values (5.8, 6.5 and 7.4) in PBS buffer solution and extended time interval in turn with 1, 2, 4, 8, 12, 24, 48, 72 and 96 h. As shown in Fig. 2B, the Ce6-GSH-AuNFs showed burst releases of Ce6 in 12 h, in which the accumulated releases were $75.7\% \pm 5.3\%$ (pH=5.8), $57.6\% \pm 5.8\%$ (pH=6.5) and $54.8\% \pm 6.8\%$ (pH=7.4). After 96 h, the Ce6 accumulated release amount at pH 5.8 was approximately $87.4\% \pm 5.8\%$, while $68.0\% \pm 3.3\%$ at pH 6.5 and $64.0\% \pm 3.1\%$ at pH 7.4. However, when wrapped by PDA layer, the burst releases of Ce6 from PDA-Ce6-GSH-AuNFs in the beginning 12 h were $25.8\% \pm 3.9\%$, $43.6\% \pm 4.2\%$ and $73.6\% \pm 6.8\%$, respectively, under the pH value of 5.8, 6.5 and 7.4 (Fig. 2C). Meanwhile, the Ce6 accumulated release amounts of PDA-Ce6-GSH-AuNFs in 96 h were $31.4\% \pm 4.5\%$, $51.0\% \pm 4.3\%$, and $82.4\% \pm 4.5\%$, which were significant lower than that of the Ce6-GSH-AuNFs group. The Ce6 accumulated release rate was affected by pH value, and the existence of PDA layer slowed the release of Ce6 under acid conditions. This attributed to the zwitterionic property of PDA, which became less negative at lower pH, thus reducing the electrostatic repulsion by the negatively charged Ce6 molecule owing to deprotonation of the pendant carboxyl groups.³⁶ Under acid conditions, the Ce6 release of PDA-Ce6-GSH-AuNFs was slower and more stable.

Photothermal effect of PDA-Ce6-GSH-AuNFs

Different light-doses (0.5, 1, 1.5 and 2 W/cm^2) for the photothermal effect of PDA-Ce6-GSH-AuNFs were studied (Fig. S10, ESI†). When the light-dose was below 2 W/cm^2 , the temperature of PDA-Ce6-GSH-AuNFs solution could not reach above $45 \text{ }^\circ\text{C}$ after 10 min laser; therefore, 2 W/cm^2 light dose was chosen in the following experiments. The photothermal efficiency of PDA-Ce6-GSH-AuNFs was 23.6%, which was higher than AuNFs (16.4%) under the same condition of photothermal measurements. Furthermore, the photothermal conversion effects of PDA-Ce6-GSH-AuNFs, AuNFs, and PBS were examined by irradiation with an 808 nm laser (2 W/cm^2). As shown in Fig. 3A and C, when irradiated with the laser, all samples exhibited a more significant increase in temperature than water. PDA-Ce6-GSH-AuNFs showed a significant temperature rise from 26.5 to $50.7 \text{ }^\circ\text{C}$, while AuNFs showed the

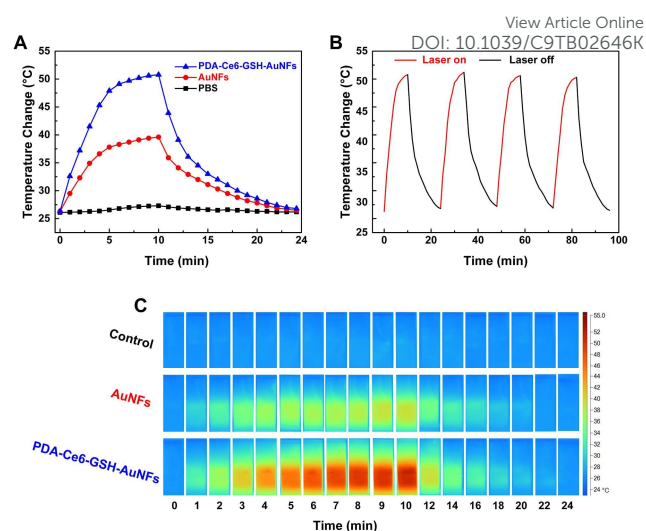


Fig. 3 Photothermal effect evaluations (A) Temperature elevation of aqueous solutions of PBS, AuNFs and PDA-Ce6-GSH-AuNFs (at the same concentration of AuNFs, $200 \mu\text{g/mL}$) exposed to laser irradiation (2 W/cm^2) for 10 min, followed by natural cooling with the laser turned off. (B) Temperature variations of a PDA-Ce6-GSH-AuNFs solution ($200 \mu\text{g/mL}$ AuNFs) over 4 cycles of continuous irradiation (2 W/cm^2). (C) Thermographic of 2 mL PBS, AuNFs and PDA-Ce6-GSH-AuNFs ($200 \mu\text{g/mL}$ AuNFs) in a 10-mm quartz cuvette exposed to laser irradiation (2 W/cm^2) for 10 min, followed by natural cooling with the laser turned off in the next 14 min.

temperature rise from 26.5 to $39.1 \text{ }^\circ\text{C}$ in 10 min. By contrast, the two samples were subsequently cooled down for 14 min. According to a previously reported model,⁵³ the photothermal efficiency (η) of AuNFs and PDA-Ce6-GSH-AuNFs was also calculated by the time constant for heat transfer (Fig. S11, ESI†). The η value of AuNFs was 16.4%, while the η value of PDA-Ce6-GSH-AuNFs was 23.6%. The PDA-Ce6-GSH-AuNFs showed higher photothermal conversion efficiency. The reason is that PDA had strong absorption in the NIR region, and the nanocoating of PDA enhances the photothermal efficiency of AuNFs.⁵⁴ In Fig. 3B, the photostability of PDA-Ce6-GSH-AuNFs was also examined after being exposed to repeated laser pulses. After four repeated lasers on/off cycles, there was no decrease in the temperature elevation. The results demonstrated that PDA-Ce6-GSH-AuNFs exhibiting excellent photostability under 808 nm NIR laser irradiation.

Cell uptake of PDA-Ce6-GSH-AuNFs examined by CLSM and TEM

$10 \mu\text{g/mL}$ Ce6-GSH-AuNFs were incubated with HeLa cells for different times: 15, 30, 60 and 120 min, then stained by Hoechst 33342 and examined by CLSM to investigate the cellular uptake. In Fig. 4A, the particles of PDA-Ce6-GSH-AuNFs were found entered into the cells incubating for 15 min, and most of them in the cytoplasm could be observed in the merged figure. When the incubation time reached 30 min, most of the cytoplasm was filled with PDA-Ce6-GSH-AuNFs, and the nuclei were still clearly apparent. After 60 min incubation, the cytoplasm of the cells was full of PDA-Ce6-GSH-AuNFs, which was similar to the case at 120 min. The results indicated that the PDA-Ce6-GSH-AuNFs might be taken up by the cells through endocytosis process, which was quite different from the diffusion mode of free drug.⁵⁵

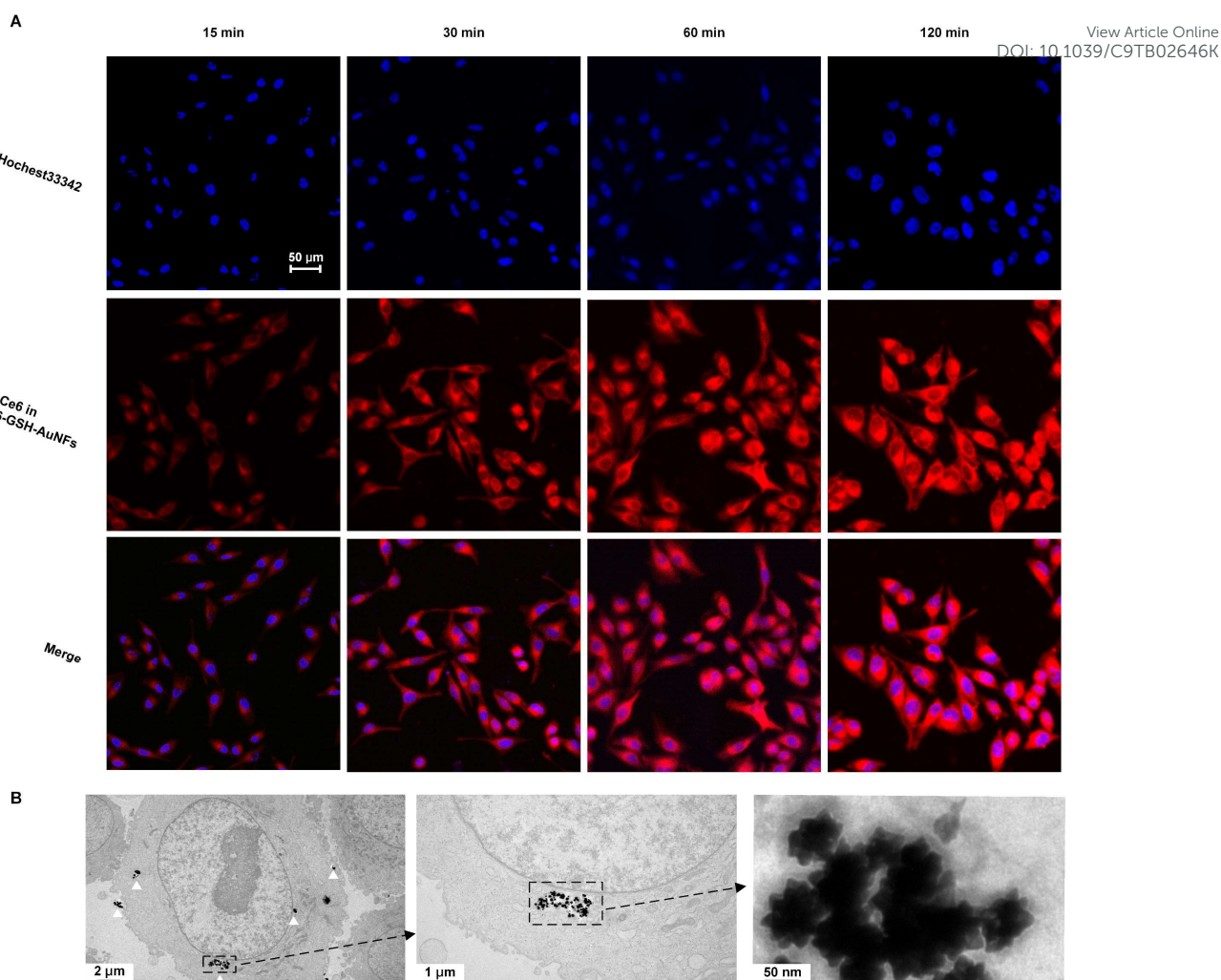


Fig. 4 Cell uptake behaviour examination of PDA-Ce6-GSH-AuNFs (A) 10 $\mu\text{g}/\text{mL}$ of sample incubated with HeLa cells investigated by CLSM, incubated for 15, 30, 60 and 120 min. The nuclei of HeLa cells were stained with Hoechst 33342. (B) The endocytosis of nanoparticles in HeLa cells investigated by Bio-TEM after 4 h incubation.

Furthermore, the endocytosis of PDA-Ce6-GSH-AuNFs in HeLa cells was investigated by Bio-TEM. PDA-Ce6-GSH-AuNFs was detected in the cytoplasm of HeLa cells after 4 h incubation (Fig. 4B). This result demonstrated that the particles of PDA-Ce6-GSH-AuNFs could be internalized into cells through the way of endocytosis, and thereby loaded Ce6 was efficiently delivered into cells.

Cell viability and the PTT & PDT effects *in vitro*

Although gold nanoparticles are low toxicity to cells, the relationship between the dosage of AuNFs and cytotoxicity should be taken into consideration. The cytotoxicity of AuNFs and PDA-Ce6-GSH-AuNFs was evaluated by MTT assay, as shown in Fig. 5A. Different concentrations of AuNFs (5, 10, 20, 50, 100 and 200 $\mu\text{g}/\text{mL}$) and PDA-Ce6-GSH-AuNFs (the same concentration of AuNFs as the AuNFs group) were incubated with L929 cells. After incubation for 48 h, the two groups showed low toxicity to L929 cells. For the high concentration of 200 $\mu\text{g}/\text{mL}$, the cell viability of the AuNFs group was a little lower than 80%, while the PDA-Ce6-GSH-AuNFs was approximately 90%. These results demonstrated that the

cytotoxicity of AuNFs could be reduced obviously after modified with thin PDA layer.

In Fig. 5B, when laser irradiation combined with PDT and PTT (660 nm, 100 mW/cm^2 , and 808 nm, 2 W/cm^2), the cell viability of PDA-Ce6-GSH-AuNF-treated HeLa cells was dramatically decreased. The cell viability declined to 13% under Ce6 concentration of 5 $\mu\text{g}/\text{mL}$, which exhibited excellent synergistic PTT and PDT effect of PDA-Ce6-GSH-AuNFs. By

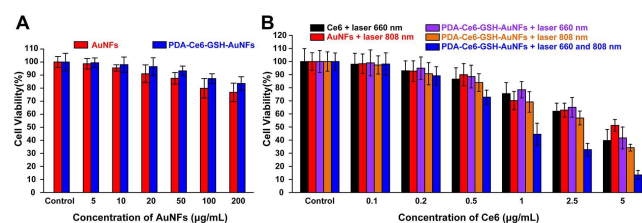


Fig. 5 Evaluation of cell viability and PTT and PDT effects. (A) Cytotoxicity of AuNFs and PDA-Ce6-GSH-AuNFs (at the same concentration of AuNFs, 5, 10, 20, 50, 100 and 200 $\mu\text{g}/\text{mL}$) against L929 (B) Cell viability of HeLa cells treated with different concentration (at the same concentration of Ce6, 0.1, 0.2, 0.5, 1, 2.5 and 5 $\mu\text{g}/\text{mL}$) of Ce6, AuNFs and PDA-Ce6-GSH-AuNFs under PDT treatment (660 nm, 100 mW/cm^2), PTT treatment (808 nm, 2 W/cm^2) or combined PTT and PDT treatment, respectively. (mean \pm SD, $n = 6$).

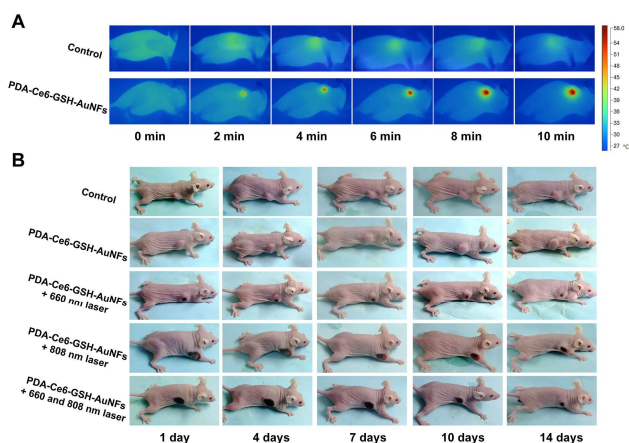


Fig. 6 PTT and PDT *in vivo* performed on mice (A) Thermal-graphic images of tumour-bearing BALB/c mice injected intratumorally with PBS or PDA-Ce6-GSH-AuNFs under 808 nm laser (2 W/cm^2) at 0, 2, 4, 6, 8 and 10 min. (B) *In vivo* therapeutic response to PDT (660 nm, 100 mW/cm^2), PTT (808 nm, 2 W/cm^2) treatment, and combined PDT/PTT treatment after 1, 4, 7, 10 and 14 days.

contrast, laser irradiation with PDT alone, PDA-Ce6-GSH-AuNFs showed the cell viability decreasing to 43% at the same Ce6 concentration, which was a little higher than the cells treated with free Ce6 (37%) due to the lower reactive oxygen species (ROS) generation in the PDA-Ce6-GSH-AuNFs. Under the same sample concentration and laser irradiation conditions as in the case of AuNFs, the cell viability of PDA-Ce6-GSH-AuNFs was 34%, while the AuNFs group was 51%. These results demonstrated that PDA-Ce6-GSH-AuNFs had a higher photothermal efficiency than AuNFs, and the synergistic PDT and PTT effect achieved by PDA-Ce6-GSH-AuNFs demonstrated excellent activity for killing the cancer cells *in vitro*.

Photodynamic/Photothermal therapy *in vivo*

The PTT and PDT combination therapeutic efficacy of the PDA-Ce6-GSH-AuNFs was further examined with tumour-bearing BALB/c mice *in vivo*. The temperature of the tumour site *in vivo* can be increased over $55 \text{ }^\circ\text{C}$, under which tumour cells can be killed when exposed to an 808 nm laser (2 W/cm^2) for 10 min. Therefore, the combination of PDT and PTT would provide an excellent synergetic effect on cancer treatment. The individual 808 nm laser-induced temperature changes of tumour sites were investigated. As shown in Fig. 6A, upon the 808 nm laser irradiation, the local temperature of the PDA-Ce6-GSH-AuNFs injected tumour rapidly increased over $55 \text{ }^\circ\text{C}$, which is sufficiently high to ablate the malignant cells. In comparing with the control group, the temperature was $35.5 \text{ }^\circ\text{C}$ for 10 min.

Furthermore, we investigated the PTT and PDT synergistic therapeutic efficacy of PDA-Ce6-GSH-AuNFs *in vivo*. There were four group mice that received different treatments, and the changes in the tumour volumes were monitored and recorded for 14 days (as mentioned in the Experimental Section). The mice experienced rapid growth of tumour volume in the control group and PDA-Ce6-GSH-AuNFs without laser group [Fig. 6B and S12, (ESI[†])], which indicated that only the injection of PDA-Ce6-GSH-AuNFs did not influence tumour growth. However, the PDA-Ce6-GSH-AuNFs groups with laser irradiation showed

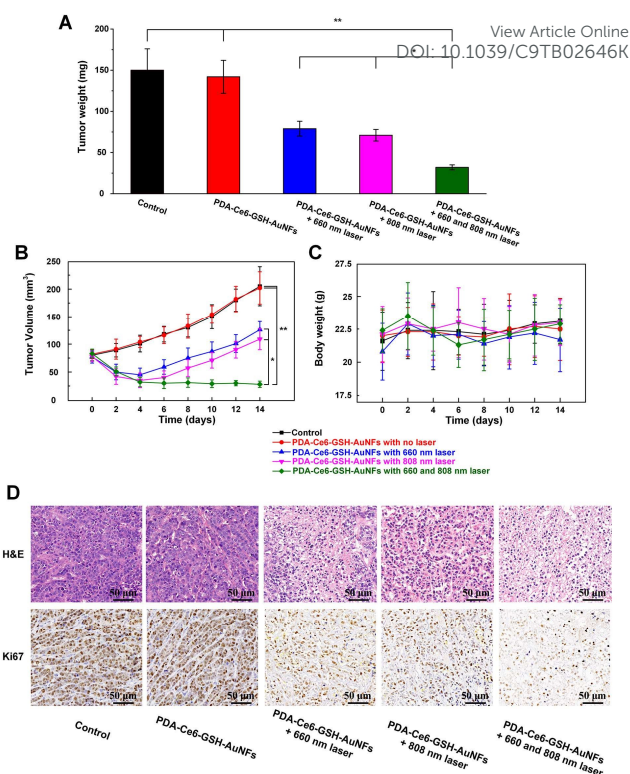


Fig. 7 (A) The weights of excised tumours from HeLa tumour-bearing mice after different treatments as indicated (mean \pm SD, $n = 3$). (B) Tumour volumes of mice after different treatments (data are presented as mean \pm SD, $n = 4$, $*P < 0.05$, $**P < 0.01$). (C) Body weight of mice in different groups after treatment (mean \pm SD, $n = 4$). (D) H&E staining and immunohistochemical staining of the excised tumours from mice after different treatments.

phototherapeutic effects, and laser irradiation significantly delays tumour growth after 14 days. Moreover, it was noteworthy that the synergistic 660 and 808 nm laser irradiation group exhibited much higher therapeutic efficiency, compared with 660 or 808 nm alone laser group on day 14, and the tumours in combined 660 and 808 nm laser group almost fully suppressed tumour growth after two weeks of treatment (Fig. 6B and Fig. 7B).

The tumours were weighed on day 14 (Fig. 7A). The synergistic 660 and 808 nm laser group exhibited 87.0% inhibition of tumour growth, whereas the 660 nm laser group and 808 nm group exhibited inhibition rates of 41.9% and 44.0%, respectively. These results demonstrate that better tumour ablation efficacy of PDA-Ce6-GSH-AuNFs was achieved by the combination of PTT and PDT, which enhanced the effects of cancer therapy. Allowing for high toxicity usually results in body weight loss. We also weighted the mice of all groups during the period of treatment, and no weight loss was obviously observed (Fig. 7C). These results indicated that the toxicity or side effects of our nano-drug carrier system were acceptable.

In addition, the antitumor efficacy was evaluated by H&E staining of tumour tissues. As shown in Fig. 7D, in 660 and 808 nm laser irradiation group, no necrosis or apoptosis was observed in the tumour tissue slices, and the tumour cells retained their normal morphology with a distinguishable membrane and nuclear structure. A certain degree of cell death and tissue

damage was found in tumours received single PDT or PTT treatment. When combined PDT and PTT in cancer treatment, the enhanced cell destruction efficacy and extensive cancer tissue damaged areas were found, as indicated by the loss of tissue architectures and decreased overall intensity of tissues. Meanwhile, the antigen Ki67 in immunohistochemistry (IHC) stained tumour sections was significantly positive expressed in the control groups, as indicated by the brown granules in the cell nucleus. However, the signal in the tumour received the combined PDT and PTT treatment (660 and 808 nm laser irradiation group) was much weaker compared with other groups. These results confirmed that PDA-Ce6-GSH-AuNFs could serve as a combined PTT and PDT therapeutic agent for enhanced cancer therapy.

Conclusion

In summary, we successfully prepared PDA-Ce6-GSH-AuNFs for combined PDT and PTT. The AuNFs possessing rich branches were prepared through a template-free method, in which HAuCl₄ was reduced by 10 μL ascorbic acid (5 mM) at 0 °C to make Au seeds, and subsequently reduced by NH₂OH·HCl. The loading content of Ce6 was approximately 14.0 wt. % with the aid of GSH. Singlet oxygen generation was about 91.0% of free Ce6. The PDA layer had an average thickness of ~10 nm, which made a remarkable redshift of ~80 nm for AuNFs and much lower toxicity of PDA-Ce6-GSH-AuNFs. The photothermal efficiency value (η) of PDA-Ce6-GSH-AuNFs was 23.6%, which was 7.0% higher than AuNFs. The antitumor efficiency of the PDA-Ce6-GSH-AuNFs upon NIR laser irradiation was also evaluated both *in vitro* and *in vivo*, and the results demonstrated that antitumor efficiency could be significantly enhanced by the combination treatment of PTT and PDT using 660 and 808 nm laser irradiation. Therefore, PDA-Ce6-GSH-AuNFs is a dual-modal phototherapy agent to achieve combined PTT and PDT treatment, and it holds promise for cancer therapy in practice.

Conflicts of interest

There are no conflicts to declare.

Acknowledgements

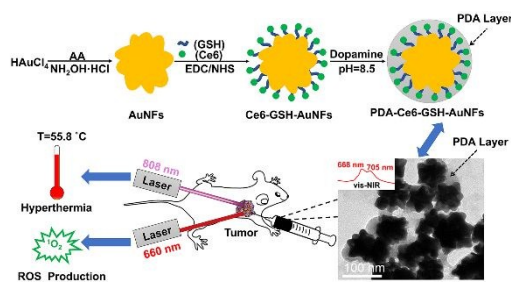
This work was jointly supported by National Natural Science Foundation of China (51373099) and Transformation Medicine Interdisciplinary Research Fund (ZH2018ZDA18) from Shanghai Jiao Tong University.

References

- 1 L. Sun, L. X. Chen and H. Li, *Int. Immunopharmacol.*, 2019, 67, 160-175.
- 2 D. N. Khalil, E. L. Smith, R. J. Brentjens and J. D. Wolchok, *Nat. Rev. Clin. Oncol.*, 2016, 13, 273-290.
- 3 Q. C. Xiao, J. Wu, X. Pang, Y. Jiang, P. Wang, A. W. Leung, L. Q. Gao, S. Jiang and C. S. Xu, *Curr. Med. Chem.*, 2018, 25, 839-860. DOI: 10.1039/C9TB02646K
- 4 P. Liu, C. Yue, Z. Sheng, G. Gao, M. Li, H. Yi, C. Zheng, B. Wang and L. Cai, *Polym. Chem.*, 2014, 5, 874-881.
- 5 W. X. Hou, F. F. Xia, C. S. Alves, X. Q. Qian, Y. M. Yang and D. X. Cui, *ACS Appl. Mater. Inter.*, 2016, 8, 1447-1457.
- 6 X. Y. Yang, Y. D. Wang, Y. H. Shi, J. H. Zou, Q. S. Zhao, Q. Zhang, W. Huang, J. J. Shao, X. J. Xie and X. C. Dong, *ACS Appl. Mater. Inter.*, 2018, 10, 12431-12440.
- 7 J. J. Dang, H. Ye, Y. J. Li, Q. J. Liang, X. D. Li and L. C. Yin, *Biomaterials*, 2019, 223, 119463.
- 8 S. L. Gai, G. X. Yang, P. P. Yang, F. He, J. Lin, D. Y. Jin and B. G. Xing, *Nano Today*, 2018, 19, 146-187.
- 9 S. Kossatz, J. Grandke, P. Couleaud, A. Latorre, A. Aires, K. Crosbie-Staunton, R. Ludwig, H. Daehring, V. Ettl, A. Lazaro-Carrillo, M. Calero, M. Sader, J. Courty, Y. Volkov, A. Prina-Mello, A. Villanueva, A. Somoza, A.L. Cortajarena, R. Miranda and I. Hilger, *Breast Cancer Res.*, 2015, 17, 66.
- 10 H. J. Kwon, Y. Byeon, H. N. Jeon, S. H. Cho, H. D. Han and B. C. Shin, *J. Control Release*, 2015, 216, 132-139.
- 11 K. K. Wang, Y. F. Zhang, J. Wang, A. Yuan, M. J. Sun, J. H. Wu and Y. Q. Hu, *Sci. Rep-UK*, 2016, 6, 27421.
- 12 X. B. Meng, K. Wang, L. Lv, Y. Zhao, C. Sun, L. J. Ma and B. Zhang, *Part. Part. Syst. Char.*, 2019, 36, 1900015.
- 13 Y. S. Shi, S. N. Liu, Y. Liu, C. Q. Sun, M. Y. Chang, X. Y. Zhao, C. L. Hu and M. L. ACS *Appl. Mater. Inter.*, 2019, 11, 12321-12326.
- 14 T. K. Ryu, S. W. Baek, R. H. Kang, K. Y. Jeong, D. R. Jun and S. W. Choi, *J. Control Release*, 2018, 270, 237-245.
- 15 L. Zhao, T. H. Kim, J. C. Ahn, H. W. Kim and S. Y. Kim, *J. Mater. Chem. B.*, 2013, 1, 5806-5817.
- 16 P. Xu, Y. Jia, Y. Yang, J. Chen, P. Hu, Z. Chen and M. Huang, *J. Med. Chem.*, 2017, 60, 8667-8672.
- 17 S. Yan, Q. Huang, J. Chen, X. Song, Z. Chen, M. Huang, P. Xu and J. Zhang, *Int. J. Nanomed.*, 2019, 14, 6799-6812.
- 18 Y. Jia, J. Li, J. Chen, P. Hu, L. Jiang, X. Chen, M. Huang, Z. Chen and P. Xu, *ACS Appl. Mater. Interfaces*, 2018, 10, 15369-15380.
- 19 P. Ghosh, G. Han, M. De, C. K. Kim and V. M. Rotello, *Adv. Drug Deliv. Rev.*, 2008, 60, 1307-1315.
- 20 X. Yang, M. X. Yang, B. Pang, M. Vara and Y. N. Xia, *Chem. Rev.*, 2015, 115, 10410-10488.
- 21 K. Niikura, N. Lyo, Y. Matsuo, H. Mitomo and K. Ljro, *ACS Appl. Mater. Inter.*, 2013, 5, 3900-3907.
- 22 J. Chen, in *Cancer Theranostics*. Ed. X. Chen and S. Wong, Academic Press, Salt Lake City, 2014, 18, 327-346.
- 23 C. Liu, L. J. Luo, L. Y. Zeng, J. Xing, Y. Z., Xia, S. Sun, L. Y. Zhang, Z. Yu, J. L. Yao, Z. S. Yu, O. U. Akakuru, M. Saeed and A. G. Wu, *Small*, 2018, 14, 1801851.
- 24 J. Lin, S. J. Wang, P. Huang, Z. Wang, S. H. Chen, G. Niu, W. W. Li, J. He, D. X. Cui, G. M. Lu, X. Y. Chen and Z. H. Nie, *ACS Nano*, 2013, 7, 5320-5329.
- 25 P. Huang, J. Lin, S. J. Wang, Z. J. Zhou, Z. M. Li, C. L. Zhang, X. Y. Yue, G. Niu, M. Yang, D. X. Cui and X. Y. Chen, *Biomaterials*, 2013, 34, 4643-4654.
- 26 N. Li, P. X. Zhap and D. Astruc, *Angew. Chem. Int. Ed.*, 2014, 53, 1756-1789.

- 27 C. Zhang, X. Cheng, M. K. Chen, J. Sheng, J. Ren, Z. Y. Jiang, J. F. Cai and Y. Hu, *Colloids Surf. B*, 2017, 160, 345-354.
- 28 Y. Y. Jian, Z. J. Deng, D. Yang, X. Deng, Q. Li, Y. L. Sha, C. H. Li and D. S. Xu, *Nano Res.*, 2015, 8, 2152-2161.
- 29 S. Kumari and R. P. Singh, *Int. J. Biol. Macromol.*, 2012, 50, 878-883.
- 30 J. Han, J. R. Li, W. F. Jia, L. M. Yao, X. Q. Li, L. Jiang and Y. Tian, *Int. J. Nanomed.*, 2014, 9, 517-526.
- 31 Q. L. Cui, X. Y. Wang, B. H. Xia and L. D. Li, *ACS Appl. Mater. Inter.*, 2013, 5, 213-219.
- 32 S. J. Wang, O. Huang, L. M. Nie, R. J. Xing, D. B. Liu, Z. Wang, J. Lin, S. H. Chen, G. Niu, G. M. Lu and X. Y. Chen, *Adv. Mater.*, 2013, 25, 3055-3061.
- 33 Y. Wang and W. Dong, *Mater. China*, 2019, 5, 470-477.
- 34 H. Lee, S. M. Dellatore, W. M. Miller and P. B. Messersmith, *Science*, 2007, 318, 426-430.
- 35 X. Liu, J. Cao, H. Li, J. Li, Q. Jin, K. Ren and J. Ji, *ACS Nano*, 2013, 7, 9384-9395.
- 36 B. Poinard, S. Kamaluddin, A. Q. Q. Tan, K. G. Neoh and J. C. Y. Kah, *ACS Appl. Mater. Inter.*, 2019, 11, 4777-4789.
- 37 B. Poinard, S. Z. Y. Neo, E. L. L. Yeo, H. P. S. Heng, K. G. Neoh and J. C. Y. Kah, *ACS Appl. Mater. Inter.*, 2018, 10, 21125-21136.
- 38 B. N. Khlebtsov, A. M. Burov and N. G. Khlebtsov, *Appl. Mater. Today*, 2019, 15, 67-76.
- 39 Q. Xu, X. Y. Guo, L. Xu, Y. P. Ying, Y. Wu, Y. Wen and H. F. Yang, *Sens. Actuat. B*, 2017, 241, 1008-1013.
- 40 Y. Y. Jiang, X. J. Wu, Q. Li, J. J. Li and D. S. Xu, *Nanotechnology*, 2011, 22, 385601.
- 41 Y. S. Luo, X. H. Ji, J. Q. Zhuang and W. S. Yang, *Colloids Surf. A*, 2014, 463, 28-36.
- 42 W. S. Saw, M. Ujihara, W. Y. Chong, S. H. Voon, T. Imae, L. V. Kiew, H. B. Lee, K. S. Sim and L. Y. Chung, *Colloids Surf. B*, 2018, 161, 365-374.
- 43 A. Mirzaie, M. Hasanzadeh and A. Jouyban, *Int. J. Biol. Macromol.*, 2019, 123, 1091-1105.
- 44 X. Zhang, N. Bao, X. L. Luo and S. N. Ding, *Biosensors. Bioelectron.*, 2018, 114, 44-51.
- 45 Z. W. Zhang, J. Jia, Y. Q. Lai, Y. Y. Ma, J. Weng and L. P. Sun, *Bioorg. Med. Chem.*, 2010, 18, 5528-5534.
- 46 C. Garrido, B. E. Weiss-Lopez and M. M. C. Vallette, *Spectrosc. Lett.*, 2016, 49, 11-18.
- 47 A. K. Tummanapelli and S. Vasudevan, *J. Phys. Chem. B*, 2015, 119, 15353-15358.
- 48 J. Choi, S. E. Lee, J. S. Park and S. Y. Kim, *Biotechnol. Bioeng.*, 2018, 115, 1340-1354.
- 49 J. W. Fu, Z. H. Chen, M. H. Wang, S. J. Liu, J. H. Zhang, J. N. Zhang, R. P. Han and Q. Xu, *Chem. Eng. J.*, 2015, 259, 53-61.
- 50 O. L. Gladkova, M. V. Parkhats, A. N. Gorbachova and S. N. Terehov, *Spectrochim. Acta. Part A*, 2010, 76, 388-394.
- 51 J. Gil-Tomas, L. Dekker, N. Narband, I. P. Parkin, S. P. Nair, C. Street and M. Wilson, *J. Mater. Chem.*, 2011, 21, 4189-4196.
- 52 W. F. Chen, M. Qin, X. Y. Chen, Q. Wang, Z. R. Zhang and X. Sun, *Theranostics*, 2018, 8, 2229-2241.
- 53 Y. Liu, K. Ai, J. Liu, M. Deng, Y. He and L. Lu, *Adv. Mater.*, 2013, 25, 1353-1359.
- 54 J. Li, W. J. Wang, L. Zhao, L. Rong, S. J. Lan, H. C. Sun, H. Zhang and B. Yang, *ACS Appl. Mater. Inter.*, 2015, 7, 11613-11623. DOI: 10.1039/C9TB02646K
- 55 X. Y. Yuan, B. S. Zhu, X. F. Ma, G. S. Tong, Y. Su and X. Y. Zhu, *Langmuir*, 2013, 29, 12275-12283.

Table of Contents Entry

View Article Online
DOI: 10.1039/C9TB02646K

A nanoscale system (PDA-Ce6-GSH-AuNFs) for synergistic photothermal and photodynamic therapy was successfully prepared, which exhibited high tumour inhibition efficacy.